

FRICTION INDUCED BRAKE VIBRATIONS AT LOW SPEEDS – EXPERIMENTS, STATE-SPACE RECONSTRUCTION AND IMPLICATIONS ON MODELLING

Hartmut Hetzler

Institut für Technische Mechanik
Fakultät für Maschinenbau
Universität Karlsruhe (TH)
76133 Karlsruhe, Germany

Email: hetzler@itm.uni-karlsruhe.de

Wolfgang Seemann

Institut für Technische Mechanik
Fakultät für Maschinenbau
Universität Karlsruhe (TH)
76133 Karlsruhe, Germany

Email: seemann@itm.uni-karlsruhe.de

ABSTRACT

Today, low frequency disc-brake noises are commonly explained as self-sustained stick-slip oscillations. Although, at a first glance this explanation seems reasonable, there are indices that cast doubt on it. For instance, the basic frequency of the observed oscillations does not scale with the disc-speed as it is with stick-slip oscillations and the classical model does not explain the observed ending of the vibrations beyond a certain speed.

Indeed, our experimental studies on groaning noises reveal two different vibration patterns: stick-slip vibrations at almost vanishing relative speed and a second, differing vibration pattern at low to moderate relative speeds. Yet, these two patterns produce a very similar acoustic impression.

While the experiment provides a vast amount of data, the dimension and structure of the underlying oscillation is not known *a priori* – hence, constructing phenomenological minimal models usually must rely on assumptions, e.g. about the number of DOF, etc.

Due to noise and complexity, the measured raw data did only allow for a first straight forward insight, rendering further analysis necessary. Hence, time-delay embedding methods together with a principle component analysis were used to reconstruct a pseudo-phase space together with the embedded attractor, to analyse for the system's dimension and to separate signal from noise.

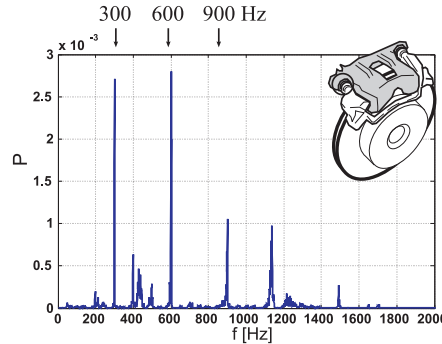


Figure 1. POWER SPECTRAL DENSITY OF THE MEASURED BRAKE NOISE ($n = 1$ rpm).

INTRODUCTION

Though being subject to intensive research over decades, vibrations of vehicle brakes are still in the scope of interest. This is because brakes can emit a broad spectrum of undesired vibrational phenomena, which may affect the convenience of car passengers and eventually lead to costly customer complaints. Often, the observed vibrations and noises are classified with respect to their frequency content and the subjective impression on human beings [1]. Roughly, two classes can be distinguished: low frequency noises in the range from 0 to 1 kHz (judder, groan, muh, howl, chatter, etc.) and high frequency noises from 1 kHz to 20 kHz (squeal).

In the past, the research efforts have concentrated on high frequency noise, which are explained as self-excited vibrations due to follower-force and eigenvalue-coupling mechanisms giving rise to system equations with non-symmetric stiffness-matrices. Concerning low frequency vibrations, one can differentiate between forced vibrations (judder), which originates e.g. from disc-thickness variations (DTV), and self-sustained oscillations (groan, muh), which are usually explained as a stick-slip phenomenon. The latter typically arise in cars with automatic gear-box, when approaching a traffic light very slowly or being manoeuvred.

The subject of this article are self-sustained low-frequency oscillations. Based on measured data, the underlying mechanisms shall be reinvestigated in order to get a deeper understanding of the processes and to allow for an appropriate modelling.

EXPERIMENTAL TEST

To investigate groaning noises of disc-brakes, experimental tests were conducted at the laboratory of the institute. The used test rig comprises a floating caliper disc-brake mounted on a front axle of a car. All tested parts were taken from series manufacturing.

Sound emission

Figure 1 shows the power spectral density (PSD) of a typical sound measurement of groaning noise from our test-rig. Independent of the motor's driving speed, the PSD shows dominant peaks at 300 Hz, 600 Hz and 900 Hz. For different speeds, the only difference in the acoustic impression is a slight shift in the timbre.

Experimental Setup

In the original setup, the brake pads – which are supposed to be somehow involved in the generation of the considered vibrations – are totally hidden under the floating caliper (Fig. 2 a). It is easily found, that the caliper – which is laterally attached to the support only by very soft elastic elements – does not contribute noteworthy to the force balance in the longitudinal (i.e. circumferential with respect to the disc) direction. In fact, the pads are entirely supported by small noses, while the caliper does only effect the normal force N on the pads (Fig. 2 b).

Therefore, to allow for a clearer view, the caliper has been removed and substituted by a screw clamp – providing the same functionality but giving direct access to the pads (Fig. 2 c). A comparison of the results before and after the replacement showed a spectrum only slightly shifted to higher frequencies (due to the reduced massed) while the groan phenomenon kept almost unchanged. Having the pads easily accessible, accelerometers were put onto their backsides as well as onto the supporting structure. In addition to these acceleration sensors,

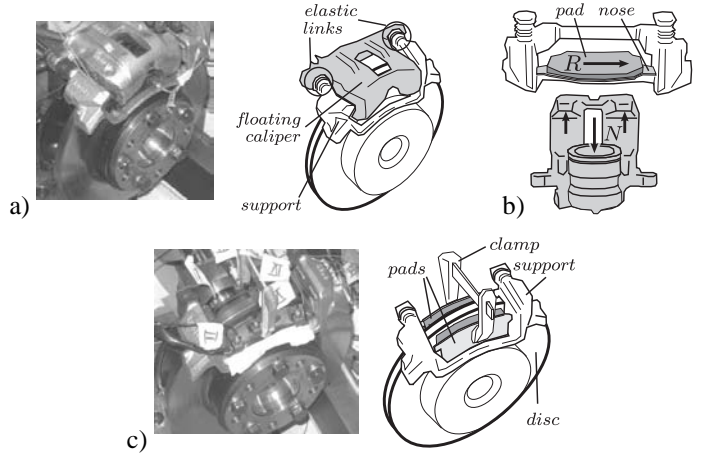


Figure 2. a) ENTIRE FLOATING CALIPER DISC-BRAKE ASSEMBLY.
b) FUNCTIONAL SCHEMATIC OF THE BRAKE ASSEMBLY.
c) REDUCED EXPERIMENTAL SETUP: CALIPER REPLACED BY A SCREW CLAMP.

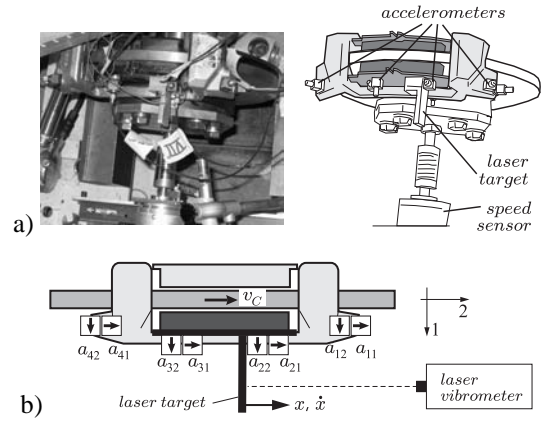


Figure 3. a) SENSOR PLACEMENT (CLAMP AND CORRESPONDING FORCE-SENSOR MISSING). b) SENSOR POSITIONS AND ORIENTATIONS.

one of the pads was equipped with a small laser target to allow for additional measurements with a laser vibrometer (Fig. 3). The tested brake assembly is driven by an electric motor (power $P = 120\text{kW}$) with the option of revolution speed or torque control. During the experiments, the choice of the control strategy did not show any effect on the observed phenomena. As well, it was analyzed whether the motor control parameters could have influence or even cause the observed phenomena.

In operation, the driving motor is certainly not able to maintain the desired nominal speed n_N (or torque) exactly. Therefore, in order to determine the actual speed v_C of the contact point as exact as possible, a rotational speed sensor as been attached

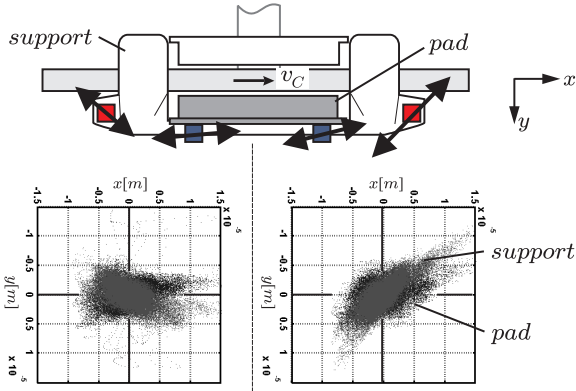


Figure 4. SPATIAL MOTION OF PADS AND SUPPORT: MEASUREMENT POINTS, DISPLACEMENTS (x - y -diagrams) AND PRINCIPLE AXES OF MOTION (DOUBLE-ARROWS).

directly to the disc, giving the actual revolution speed n_{act} .

The following experimental data refers to experiments with a normal force $F_B = 1500$ N onto the pads and a sense of rotation of the disc in positive v_C direction (cf. Fig. 3). Experimental tests with other normal forces or inverted sense of rotation did not give fundamentally new results. Though, the normal force F_B was found to have major influence on the borders between different types of vibration. The data have been recorded with a sample frequency of $f_s = 5120$ Hz.

Spatial Motion while Groaning

To get an overview on the overall spatial motion, the acceleration data have been time integrated to velocity and displacement level and band-pass filtered to remove drift and high-frequency noise. Finally, the data have been transformed from the sensor-fixed coordinate system to the inertially fixed system.

Since a comparison of the measured data from different points indicated, that elastic deformations of the involved parts are of minor order, they were considered as rigid bodies. Hence, it is possible to characterize the motion of the involved parts (e.g. the support) by means of their instantaneous centers of rotation.

Figure 4 outlines the measurement points on the support structure and on the pad, as well as the dominant directions of motion (indicated by double-sided arrows). The two diagrams below give the absolute displacement of the measurement points relative to their individual initial position. It is found, that the dominant directions of motion of the sensors on the supporting structure differ strongly from them on the pads. The support moves about an instantaneous center of rotation, which is located near to the brake, towards the driveshaft (cf. Fig. 6). This behavior may be explained by the asymmetric fixation of the brake.

In contrast, the pad's motion is dominated by translational

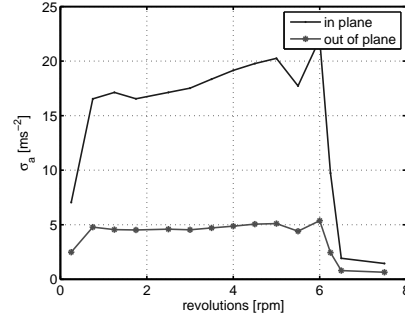


Figure 5. STANDARD DEVIATION σ_a OF THE PAD'S ACCELERATIONS IN IN-PLANE AND OUT-OF-PLANE DIRECTION.

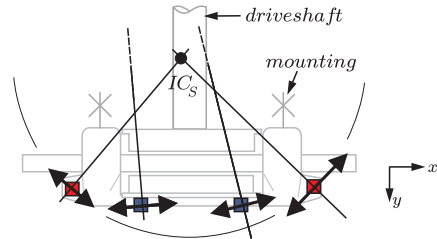


Figure 6. INSTANTANEOUS CENTERS OF ROTATION: CENTER IC_S OF THE SUPPORT'S MOTION LIES ALONGSIDE THE BRAKE, THE CENTER OF THE PAD'S MOTION IS FAR OUTSIDE THE DISPLAY.

(in-plane) motions in the y -direction. Due to the disc's sense of rotation, the pads are pressed to the right against the support: hence, following that point of the supporting structure, small lateral out-of-plane motions are superimposed to the right tips of the pads. The resulting instantaneous center of motion is situated far outside the display of Fig. 6 and thus not shown. See also figure 5 for a comparison of the pad's accelerations in in-plane and out-of-plane direction.

In-Plane Vibrations of the Brake-Pads

As shown, during groaning the pad's vibrations are dominated by longitudinal in-plane motions, i.e. along the x -direction in Fig. 3b). In the following, displacements in this direction are described by the variable x .

Figure 8 displays the displacement and velocity (x, \dot{x}) of the considered pad at different operating points with varying (nominal) driving speeds n [rpm]; the corresponding nominal contact point speed on the disc is $v_0 = r_{pad} \frac{\pi}{30} n$ [m/s].

With the revolutional speed n_{act} , the actual speed of the contact point is $v_C = r_{pad} \frac{\pi}{30} n_{act}$ [m/s]. To allow for interpretations considering the relative velocity $v_{rel} = \dot{x} - v_C$ [m/s], for each pad position x the corresponding contact point speed v_C on the disk is displayed as well.

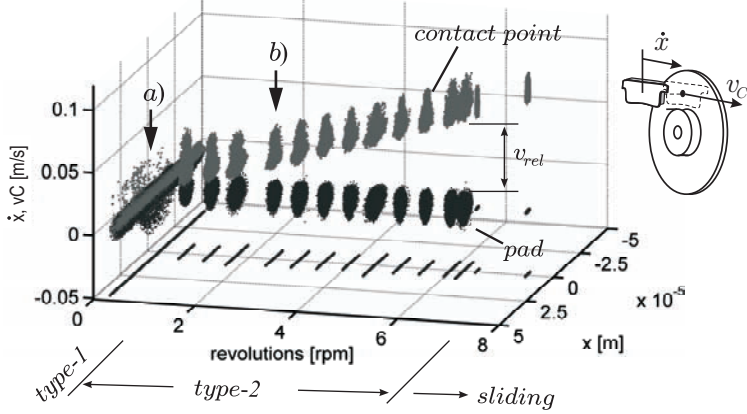


Figure 7. MEASURED STATE VARIABLES (x, \dot{x}) OF THE PAD (BLACK) AND THE CORRESPONDING SPEED OF THE CONTACT POINT (x, v_C) (GREY) ON THE DISC, PLOTTED OVER THE NOMINAL REVOLUTION SPEED [rpm] (cf. Fig. 8).

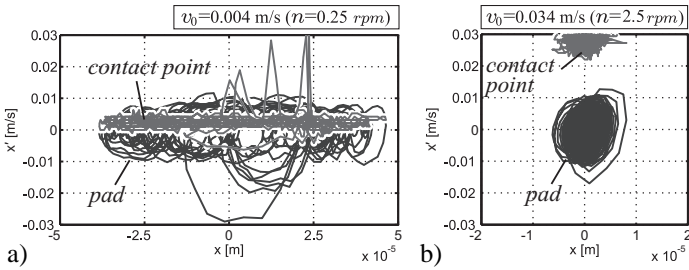


Figure 8. STATE VARIABLES (x, \dot{x}) OF THE PAD (BLACK), CORRESPONDING SPEED OF THE CONTACT POINT (x, v_C) (GREY) ON THE DISC:
a) NOMINAL SPEED OF 0.25 rpm. b) NOMINAL SPEED OF 2.5 rpm.

Apparently, the pad exhibits two different types of motion – although the acoustical impression stays almost the same and is dominated by contents at about 300 Hz, which refers to the lowest eigenfrequency of the disk. The observed vibrations may be classified as follows:

- *Type-1*: At very small driving speeds, the pad undergoes large vibrations (cf. Fig. 8 a). Since the relative speed $v_{rel} = \dot{x} - v_C$ between pad and disk vanishes in some parts of the motion, the assumption of stiction periods and therefore of some kind of stick-slip-oscillation is obvious.
- *Type-2*: At higher speeds the average contact point speed v_C scales linearly with the nominal driving speed n (cf. Fig. 7). In contrast, the pad exhibits motions of a smaller amplitude and different pattern than before (compare Fig. 8 a), b). In

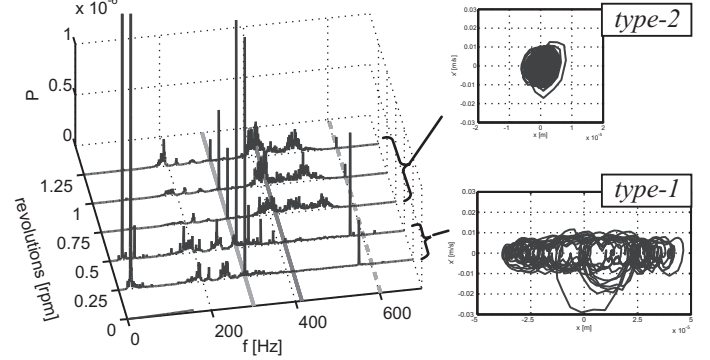


Figure 9. POWER SPECTRAL DENSITIES P_{xx} OF THE INPLANE VIBRATION OF THE PADS.

contrast to the contact point speed v_C , the pad's maximum speed does not scale with the driving speed, but stays constant over a wide range. Hence, the relative velocity v_{rel} increases with increasing driving speed, rendering the assumption of (macroscopic) stiction periods implausible. Of course, the used experimental set-up could not capture elastic deformation of the pad or microscopic dynamics of the contact (i.e. interaction of the asperities, etc.).

- *Sliding*: The groaning sound emission and the pad's vibrations can be observed up to speeds of about 6.5 rpm. At this point, vibrations cease and the brake is sliding almost silently.

This threefold behavior can be observed over a broad range of operation conditions, where borders between the different vibration types are mainly determined by the normal force F_B .

Due to the lack of any forced or parametric excitations with the observed frequencies, the underlying mechanism is assumed to be some kind of self-excitation. Hence the mechanical system is assumed to be autonomous, i.e.

$$\dot{\mathbf{z}} = \mathbf{f}(\mathbf{z}) \quad (1)$$

where $\mathbf{z} = (z_1, \dots, z_n)^T$ is the state-vector. With respect to self-excitation phenomena, the observed behaviour will be examined for periodic solutions and limit cycles.

As a first attempt to overcome the noisy character of the experimental data, the distribution density $p(x, \dot{x})$ of the measured displacements and velocities is calculated for each parameter set. Figure 10 shows three-dimensional plots of the distribution densities of the phase-plots displayed in figure 8.

Additionally, in the sense of a Poincaré section the distributions $p(x, 0)$ at $\dot{x} = 0$ are displayed. While for low speeds (e.g. 0.25 rpm, cf. Fig. 10 a) this section shows a bimodal distribution $p(x, \dot{x} = 0)$, indicating a periodic behavior, this is not the

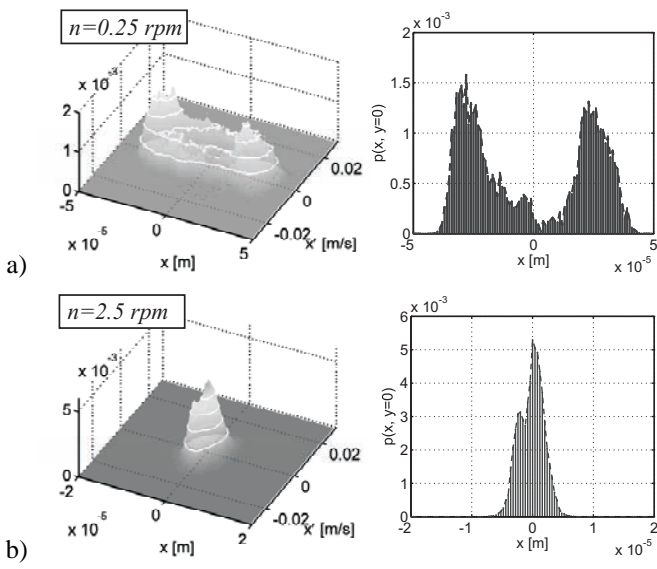


Figure 10. a) NOMINAL SPEED OF 0.25 rpm: DISTRIBUTION DENSITY OF (x, \dot{x}) (LEFT) AND POINCARÉ-SECTION AT $\dot{x} = 0$ (RIGHT). b) NOMINAL SPEED OF 2.5 rpm: DISTRIBUTION DENSITY OF (x, \dot{x}) (LEFT) AND POINCARÉ-SECTION AT $\dot{x} = 0$ (RIGHT).

case for higher speeds (e.g. 2.5 rpm, Fig. 10 b). Here $p(x, \dot{x} = 0)$ is centered, unimodal and seems gaussian. Within each domain of motion (type-1, type-2, sliding), the densities are stationary and hence independent from the driving speed speed n .

Further Analysis

The direct analysis of the measurements showed that for the first observed type of oscillations (0.25 – 0.5 rpm) the speed of the pad may reach the speed of the disc, justifying the assumption of macroscopic stick-slip oscillations. Here, the distribution density $p(x, \dot{x})$ of the in-plane state-variables stresses the existence of periodic motion.

In contrast, for the type-2 vibrations at higher speeds the pad's speed does no longer reach the surface speed. Instead, a motion establishes, that has almost constant maximum speeds for all tested parameter sets of n . Here, $p(x, \dot{x})$ does not show any periodicity at all - although permanent oscillations (without excitation from outside) are observed.

This gives rise to the question, whether the considered space – spanned by x and \dot{x} – has a sufficient dimension to contain the attractor of the self-sustained oscillation or it is only a subspace of the total state-space. Attempts to span the entire state-space using data from further measurement points on the system failed, since even then it was not possible to detect any periodicity in the measured data.

Hence, in order to get further insight into the structure of the

phenomenon, it was tried to search for the assumed limit cycle by means of a reconstruction of a pseudo state-space by a time-delay embedding method [2], [3].

Following the theorem of Ruelle & Takens, it is possible for a smooth autonomous system like (1) to construct an object in a so called pseudo-state-space, which exhibits the same topological properties as the attractor in the physical state-space: hence, it shows the same dimension, periodicity, etc. To this end, one attempts to span the pseudo-state-space by means of p linearly independent vectors. If the solution of (1) is given by $\mathbf{z}(t) = \Phi(t, \mathbf{z}_0)$, a scalar measurement can be written as

$$s(t) = \mathcal{S} \{x(t)\} = \mathcal{S} \{\Phi(t, \mathbf{z}_0)\}, \quad (2)$$

where \mathcal{S} symbolizes the sampling.

A very common choice of such basis vectors is by means of the delayed time series

$$\mathbf{y}_0(k) = [s(t_0 + k\Delta t)]^T, \quad (k = 0 \dots N), \quad (3)$$

containing N measured or simulated values (time: $k\Delta t = t$, sample period: Δt). Further series can be constructed from the measured data by a delay of j -times the time-shift τ , yielding $(p-1)$ vectors

$$\mathbf{y}_j(k) = [s(t_0 + k\Delta t + j\tau)]^T, \quad (j = 1 \dots (p-1)), \quad (4)$$

where $\tau = i\Delta t$. Hence, the task will be to choose an i which yields an appropriate set of basis vectors $\mathbf{y}_j(k)$ to span the pseudo-state-space.

In principle, scalar data are sufficient – as long as all state variables couple to each other. The reconstructed pseudo-attractor will then be related to the physical attractor by a one-to-one nonlinear mapping. This is called a *topological embedding*.

While for noise-free data the choice of the time-delays $\tau = i\Delta t$ is almost arbitrary, in the presence of noise (e.g. due to the measurement) choosing the right i will be crucial (usually Δt is given due to the measurement settings). Additionally, noise will make it difficult to recognize the correct state-space dimension d . For this, several methods have been developed to find the appropriate number i_{opt} of delays and the dimension d necessary to embed the attractor [4].

Classical embedding Basically, there are two state-of-the-art ways of choosing an i_{opt} : one way to choose i_{opt} of the delay vectors is to use some measure of the statistical or information dependency within the time series. To this end, common measures and criteria are:

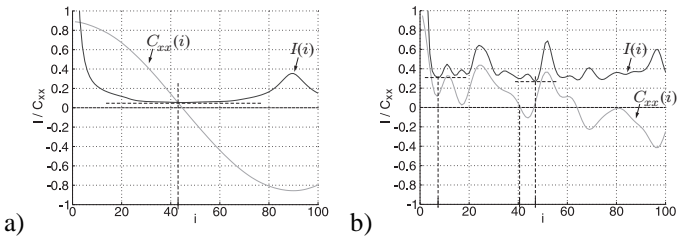


Figure 11. CHOICE OF TIME DELAY $\tau = i\Delta t$ BY ZEROCROSSING OF THE AUTOCORRELATION $C_{yy}(i)$ AND LOCAL MINIMUM OF MUTUAL INFORMATION $I(i)$:

- a) TYPE-1 VIBRATIONS: C_{yy} AND $I(i)$ SUGGEST $i_{opt} = 44$.
- b) TYPE-2 VIBRATIONS: NO DISTINCT SUGGESTION, $I(i)$ DOES NOT SHOW A CLEAR MINIMUM.

- The **Autocorrelation** $C_{yy}(i)$ is a measure for the (linear) statistical dependency between the signal $y(t)$ and the shifted signal $y(t + i\Delta t)$. Hence, a zerocrossing of $C_{yy}(i)$ indicates (linear) statistical independency of $y(t)$ and $y(t + i\Delta t)$. Usually, i_{opt} is chosen according to the first zero crossing.
- The **Average Mutual Information** $I(i)$ of two signals is defined as

$$I(i) = \sum_k p(y_0(k), y_i(k)) \log_2 \left[\frac{p(y_0(k), y_i(k))}{p(y_0(k)) p(y_i(k))} \right] \quad (5)$$

where $y_0(k) = y_0(k\Delta t)$ is the time series, $y_i(k) = y(k\Delta t + i\Delta t)$ the i -th delay vector, $p(\cdot)$ is a distribution density and $p(\cdot, \cdot)$ is a joint distribution density. Based on information theory, it gives a generalized measure of dependency between the time series y_0 and its delay vectors. Due to this general character, it is often chosen for the analysis of presumably highly-nonlinear systems. The i_{opt} is usually chosen according to the first local minimum.

Figure 11 shows the autocorrelation function $C_{yy}(i)$ and the average mutual information $I(i)$ for typical examples of type-1 and type-2 vibration. While for the first type the correlation criterion as well as the mutual information criterion yield the same suggestion for the time-shift ($i_{opt} = 44$), both criteria do not give a common hint regarding the type-2 vibrations. In particular, they do not show clear and isolated (local) minima or zero-crossings. Several attempts with the i -values suggested by each of the methods failed to give further structural informations about the state-space.

Principle Component Analysis An alternative approach starts with the construction of a so-called trajectory matrix

$$\mathbf{Y} = [\mathbf{y}_0 - \mathbf{y}_{av} | \mathbf{y}_1 - \mathbf{y}_{av} | \dots | \mathbf{y}_{(p-1)} - \mathbf{y}_{av}] , \quad (N \times p), \quad (6)$$

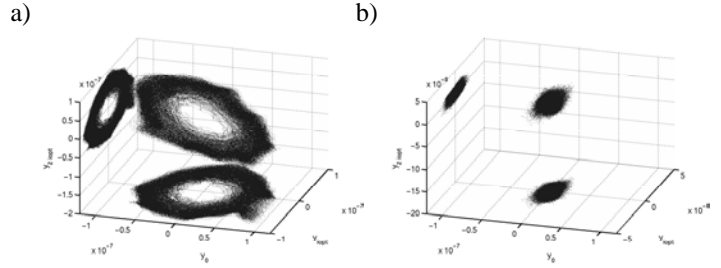


Figure 12. TIME-DELAY EMBEDDING USING i_{opt} FROM C_{yy} AND $I(i)$:

- a) TYPE-1: BOTH CRITERIA YIELD THE SAME i_{opt} , GOOD RECONSTRUCTION OF A PERIODIC ATTRACTOR.
- b) TYPE-2: THE CRITERIA DID NOT SUGGEST A COMMON i_{opt} ; TRYING EACH ONE'S SUGGESTION FAILED TO REVEAL THE MOTION'S STRUCTURE.

containing p time series of length N and delay $(p-1)$, which are centered to their average \mathbf{y}_{av} . With this, the real-valued, symmetric covariance matrix $\Sigma = \mathbf{Y}^T \mathbf{Y}$ ($p \times p$) can be calculated. The basic idea is to find the eigenvalues λ_j ($j = 1 \dots p$) and the eigenvectors \mathbf{c}_j (i.e. principle axes) of the covariance-matrix Σ and to project the the data onto these vectors, yielding the principle components

$$\Psi_j = \mathbf{Y} \mathbf{c}_j. \quad (7)$$

The original time series can be recovered as a superposition according to

$$\mathbf{y}_0 = \sum_j^p \Psi_j. \quad (8)$$

This method is referred to as principle component analysis (also: principle value decomposition, singular value analysis) and is related to the Karhunen-Loéve-Theorem [2], [5]. It plays an important role in the fields of signal processing and pattern recognition. In particular, the eigenvalue λ_j is a measure of how a principle component contributes to the reconstruction of the time-series. Hence, it can be used to distinguish noise from signal or to identify the number of (with respect to signalpower) relevant coordinates. In that latter sense, it seems promising to derive the necessary state-space-dimension and hence model dimension from it. It has to be mentioned, that λ_j gives no fool-proof hints, since eventually it is merely a measure of the energy of Ψ_j but not of the contained information. Additionally, it may be distorted for systems with time-variant structure (cf. Appendix A).

Figures 13 and 14 show the reconstructed attractors as well as the first ten of the according eigenvalues λ_j . For each domain,

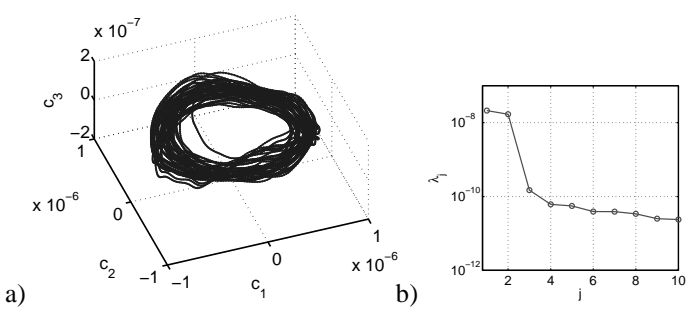


Figure 13. PCA, TYPE-1 (0.25 rpm):
a) SPACE OF THE FIRST THREE PRINCIPLE AXES c_j : RECONSTRUCTED PERIODIC ATTRACTOR.
b) SPECTRUM OF SINGULAR VALUES, INDICATING TWO DOMINANT AXES.

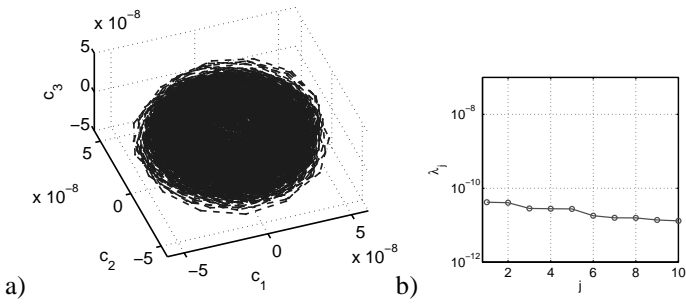


Figure 14. PCA, TYPE-2 (2.5 rpm):
a) SPACE OF THE FIRST THREE PRINCIPLE AXES c_j : NO PERIODICITY NOTICEABLE.
b) SPECTRUM OF SINGULAR VALUES: UNARTICULATED SPECTRUM INSTEAD OF DOMINANT DIRECTIONS.

only one single analysis is shown, since within a domain (type-1, type-2) the results do not differ from these exemplary displays.

While for the type-1 motion, the result already found using the conventional time-delay embedding (cf. Fig. 12) was confirmed, this method also could not reveal a clear state-space structure for the vibrations of type-2. Additionally, the eigenvalue spectrum is flat and lacks of any articulated contents. Until now, it needs to be interpreted what might be the reason.

Explanations may be:

- The relevant state-variables are not coupled adequately to the observed measurement data and hence the latter were not appropriate as data basis for reconstruction.
- The macroscopic motion of the pad results from complex dynamics (e.g. of the bristles/asperities) in the contact zone. The flat but not vanishing spectrum could then be interpreted

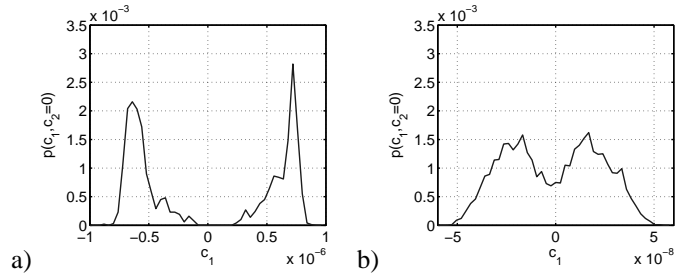


Figure 15. POINCARÉ-SECTIONS THROUGH DISTRIBUTION DENSITIES $p(c_1, c_2 = 0)$:
a) TYPE-1: CLEAR BIMODAL DISTRIBUTION DENSITY.
b) TYPE-2: SLIGHT BIMODAL CHARACTER, SUGGESTING SOME PERIODICITY.

as to be caused by a huge number of internal contact variables necessary for description. Eventually, this could motivate a stochastic description of the contact behavior.

- The vibration is mainly controlled by a component with only little energy (i.e. a small eigenvalue λ_j), but important information (e.g. like a trigger signal).
- The method per se was not able to capture the dynamics. Eventually, principle component analysis relies on the covariance matrix, which is mainly a measure of linear dependencies of the underlying system. However, the method proofed powerful with the analysis of a simple stick-slip oscillator model (cf. Appendix A).

Applicability of the Methods If one assumes stick-slip-motion during the type-1 vibrations – and therefore periods, where the underlying system is all but smooth – problems should be expected with the analysis of this very type of motion (cf. [6]). Hence, the applicability of all methods on non-smooth time-variant systems was examined with the analysis of a simple stick-slip oscillator. Details are given in Appendix A.

MECHANICAL MODELLING

Type-1 vibrations

The PCA eigenvalue spectrum of type-1 vibrations indicates (cf. Fig. 13), that the behavior is dominated by two state-space directions – i.e. one mechanical DOF. Hence, already a model with one DOF should be able to capture the basic dynamics. Indeed, even the first two principle components (c_1-c_2 in Fig. 13) as well as the classical embedding (Fig. 12) with the time series and only one delay vector show a clearly periodic solution.

The sound spectrum (1) shows articulated contents at about 300 Hz and 600 Hz, which refer to eigenfrequencies of the disc and its fixture [7]. Since the sound emission is produced by the disc, an appropriate minimal model should also incorporate the

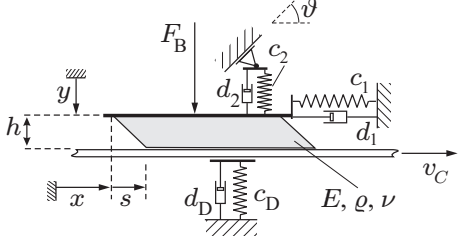


Figure 16. MINIMAL MODEL FOR TYPE-1 OSCILLATIONS.

observed coupling of the circumferential to the lateral motions and hence to the motions of the disc. Finally, considering the fact that the relative speed vanishes in some parts of the motion, the model should also incorporate the stick-slip phenomenon.

Figure 16 shows a minimal model of a shear-elastic brake pad, which is pressed onto a sliding disc (speed v_C) by a braking force F_B . The model considers the translational motion of the backplate of the pad (coordinate x), the shear-deformation between this rigid plate and the contact area to the disc, as well as the lateral displacement y of pad and disc. Obviously, the coordinate x of this model corresponds to the measured displacement x from the experiment. The support of the pad in circumferential and lateral direction is modelled by the elasticities c_1 and c_2 , while c_D accounts for the lateral stiffness of the disc. The coupling of the circumferential and lateral motions is modelled by the datum y_0 of the elasticity c_2 depending on x by $y_0 = \tan \vartheta x$. To account for dissipative effects, all elasticities are accompanied by viscous dampers.

Hamilton's Principle provides a comfortable way to derive the according ordinary and partial differential equations. Finally, using Galerkin's method a system of ordinary differential equations can be derived. With the coordinate s of the first shear-deformation mode (cf. fig. 16) and x , y the coordinates of the backplate of the pad, the state vector $\mathbf{X} = (\mathbf{x}, \mathbf{s}, \mathbf{y})^T$ is set up. Hence, in the notation of Filippov the system of differential equations reads

$$\mathbf{M}\mathbf{X}'' + \mathbf{D}\mathbf{X}' + \mathbf{K}\mathbf{X} \in \mathbf{r}\mathbf{R} \quad (9)$$

where

$$\mathbf{M} = \begin{bmatrix} 1 & \frac{1}{2} & 0 \\ \frac{3}{2} & 1 & 0 \\ 0 & 0 & 1 \end{bmatrix}, \quad \mathbf{D} = \begin{bmatrix} 2D_1 & 0 & 0 \\ 0 & 2D_2\eta & 0 \\ -2\tan\theta D_2\eta_2 & 0 & 2D_2\eta_2 + 2D_D\eta_D \end{bmatrix}$$

$$\mathbf{K} = \begin{bmatrix} 1 & 0 & 0 \\ 0 & \eta^2 & 0 \\ -\tan\theta\eta_2 & 0 & \eta_2^2 + \eta_D^2 \end{bmatrix}, \quad \mathbf{r} = \begin{bmatrix} 1 \\ \frac{3}{b} \\ 0 \end{bmatrix}.$$

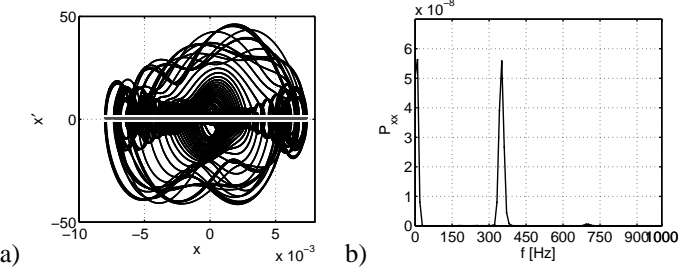


Figure 17. SIMULATION RESULTS (TYPE-1 OSCILLATIONS)
 $(\omega_1 = 2\pi \cdot 900 \text{ rad s}^{-1}, \eta = 2, \eta_D = 0.33, \eta_2 = 0.7, \tan \vartheta = 0.3, \mu_S = 0.6, \mu_k = 0.4, N = 1300 \text{ N}, v_0 = 0.5)$
a) PHASE DIAGRAMM x - x' (GREY LINE INDICATING v_0).
b) PSD P_{xx} : SPECTRUM OF IN-PLANE DISPLACEMENT x SHOWS ARTICULATED CONTRIBUTION OF THE COUPLED OUT-OF-PLANE VIBRATIONS AT ABOUT 300 Hz.

In the latter, $(\cdot)' = \frac{d}{d\tau}$ denotes derivations with respect to the dimensionless time $\tau = \omega_1 t$, where $\omega_1 = \sqrt{\frac{c_1}{m}}$ is the natural angular frequency of the circumferential motion. With the angular frequencies $\omega_2 = \sqrt{\frac{3E}{2(1+v^2)h\rho}}$ and $\omega_D = \sqrt{\frac{c_D}{m}}$, the frequency ratios $\eta = \frac{\omega_2}{\omega_1}$ and $\eta_D = \frac{\omega_D}{\omega_1}$ are introduced. The set of possible friction force R is given by

$$R = \begin{cases} \mu_k N \operatorname{sign}(v_{rel}) : v_{rel} \neq 0 \\ [-\mu_S N; \mu_S N] : v_{rel} = 0 \end{cases} \quad (10)$$

where μ_k is the kinetic friction coefficient, μ_S is the static friction coefficient, $N = F_B - c_D y$ is the contact normal force and $v_{rel} = \dot{x} + \dot{z} - v_0$ is the relative speed in the contact between disc and pad. The pad's extent is given by its height h and its width b . Its Young's modulus is given by E , its Poisson's ratio by v and its density by ρ . The total mass is m .

Figure 17 shows typical simulation results. The model is found to exhibit self-excited oscillations – sustained by the stick-slip-mechanism – which due to the coupling provoke lateral oscillations of the disc. The latter oscillations contribute significantly the spectrum P_{xx} at a frequency which is determined by η_D and η_2 . The phaseplot qualitatively resembles that one from the measurement.

Type-2 vibrations

Since the character of the type-2 vibrations is still vague, it is not yet possible to formulate clear implications on the necessary properties of a mechanical model. It shall be recalled, that the basic effect is supposed to be self-excitation. A possible mechanism could be oscillatory instability ("flutter") due to a nonsymmetric stiffness matrix, which arises from the coupling

of circumferential and lateral motions. In that case, nonlinearities have to be found, that limit the amplitudes. Another possible approach can be a stochastic friction model.

CONCLUSION

Experimental examinations on noise and vibration of vehicle disc-brakes at very low speed revealed two qualitatively totally different motion patterns: *type-1* motion exhibiting large amplitudes and vanishing relative speed between disc and pad and a second pattern (*type-2*) at non-vanishing relative speed, showing slightly smaller amplitudes which are independent of the driving speed of the disc. At a certain driving speed, the phenomenon disappears.

A direct state-space analysis of the measured data indicated periodic motion for the *type-1* vibrations which very likely includes periods of stiction. Although, it did not allow further insight into the *type-2* oscillations.

Setting-up minimal models to understand the underlying mechanisms relies on assuming a certain dimension (DOF), hence further understanding of the phenomenon is desirable. Since possibly the measured data did not suffice to reconstruct the state-space, methods of state-space reconstruction (i.e. time delay embedding) have been used to gain further insight. While this worked fine with *type-1*, the *type-2* oscillation again could not be clarified significantly. Future work will have to concentrate on this issue.

Furthermore, the spatial motion of the involved parts was analyzed, in order to derive indications on the motion kinematics and hence how to set up an appropriate minimal model. It was found, that the supporting structure follows a circular path (about an instantaneous center of motion), while the pad moves rather translational. Hence, future models will have to account for this coupling of circumferential and lateral motions.

Concluding, suggestions on the mechanical modelling are formulated. With respect to the observed type-1 oscillations, a stick-slip oscillator is presented, which also considers the shear elastic properties of the pad and the contact. A main task of future work will be to reveal the mechanism behind the *type-2* vibrations, which will involve measurement data analysis as well as studying minimal models.

Additionally, state-space reconstruction methods have been examined with the example of a simple stick-slip oscillator ("mass on a drivebelt") in order to justify the application of these methods on non-smooth systems. For the examined problem, the autocorrelation criterion failed and the criterion of minimal average mutual information gave acceptable results, while the method of principle component analysis yielded an almost perfect reconstruction.

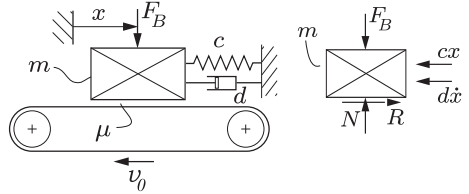


Figure 18. CONSIDERED FRICTION OSCILLATOR.

REFERENCES

- [1] Wallaschek, J., and et.al. "A survey of the present state of friction modelling in the analytical and numerical investigation of brake noise generation". *Proceedings of the ASME vibration conference, Las Vegas, 1999.*
- [2] Nayfeh, A.; Balachandran, B., 1994. *Applied nonlinear dynamics*. John Wiley & Sons, New York.
- [3] Strogatz, S., 1994. *Nonlinear Dynamics and Chaos*. Perseus Books Group, Cambridge, MA.
- [4] Casdagli, M., and Eubank, S., 1991. "State space reconstruction in the presence of noise". *Physica D*, **51**, pp. 52–98.
- [5] Sprott, J.-C., 2003. *Chaos and Time-Series Analysis*. Oxford University Press, Oxford, UK.
- [6] Feeny, B., and Liang, J., 1997. "Phase-space reconstruction and stick-slip". *Nonlinear Dynamics*, **13**, pp. 39–57.
- [7] Hetzler, H., and Seemann, W., 2005. "On low frequency disc-brake vibrations". *Proceedings in Applied Mathematics and Mechanics (PAMM)*, **5**(1), pp. 95–96.

Appendix A: On state-space reconstruction for non-smooth, self-excited systems of variable structure

One of the main fundamentals of state-space reconstruction is the theorem of Ruelle & Takens, which unfortunately assumes a smooth system behind the considered time-series. Despite the vast literature on state-space reconstruction, there is only little work on non-smooth systems of variable structure, especially systems exhibiting stick-slip motion. As an example, the classical "block-on-a-drivebelt" shall be examined, where the force in the contact may either be sliding friction F_k or a stiction force F_S . Using the Filippov-notation, the equation of motion reads

$$\ddot{x} + 2D\omega_0\dot{x} + \omega_0^2x \in \frac{1}{m}R, \quad R = \begin{cases} [-\mu_0N; +\mu_0N] : v_{rel} = 0 \\ \text{sign}(w)\mu N : v_{rel} \neq 0 \end{cases}, \quad (11)$$

with the relative velocity $v_{rel} = v_0 - \dot{x}$, the dimensionless damping measure $D = \frac{d}{2m\omega_0}$, the natural angular frequency $\omega_0 = \sqrt{\frac{c}{m}}$ of the undamped system and the normal contact force N . Figure 19 shows the phase-diagram (x, \dot{x}) and the displacement $x(t)$: the motion exhibits a period of pure sliding, which is followed by a period of stiction. During sliding, the system is described by a

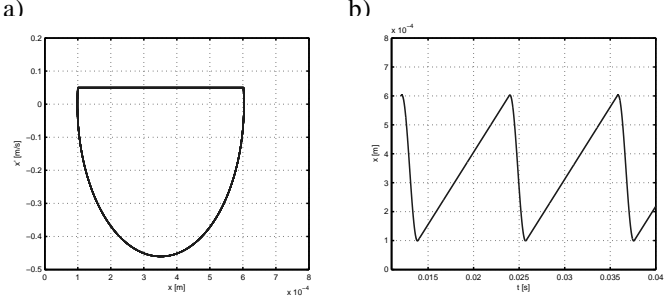


Figure 19. STICK-SLIP OSCILLATOR:
a) THEORETICAL PHASE-PLOT. b) DISPLACEMENT.

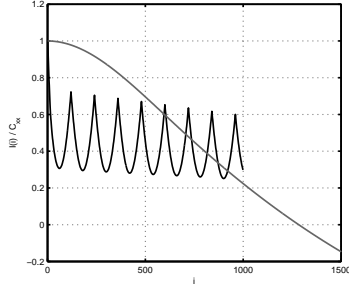


Figure 20. CORRELATION $C_{yy}(i)$ AND AVERAGE MUTUAL INFORMATION $I(i)$. THE ZEROCROSSING OF C_{yy} IS AT ABOUT $i_1 = 1300$, THE FIRST MINIMUM OF $I(i)$ AT $i_2 = 60$.

two state variables (1 DOF), while during the stiction period the mass has 0 DOF (due to the kinematic constraint $\dot{x} = v_0$). Obviously, this system exhibits non-smooth behaviour and its structure varies during the motion. One example is given in [6]: there it was found for the harmonically driven stick-slip oscillator, that the reconstruction may "collaps", i.e. contain intersections. To cope with this, the phase of the excitation was used, which in our case is not possible due to the lack of an excitation.

As described earlier, two standard ways of choosing an appropriate time delay are the criteria of vanishing autocorrelation $C_{yy}(i)$ or minimum of the mutual information function $I(i)$. Figure 20 shows both functions (normalized to their maximum) for the limit-cycle displayed in Fig. 19. Obviously, both criteria suggest strongly differing values of i .

Figure 21 shows the resulting reconstructions, according to the suggestions of either criterion. Choosing the time delay $i_1 = 1300$ from the autocorrelation criterion does not yield an acceptable reconstruction of the the limit-cycle: the trajectory intersects (which is not possible with an autonomous system) and the reconstruction suggests two stiction periods (straight lines). In contrast, the delay $i_2 = 60$ from the mutual information criterion

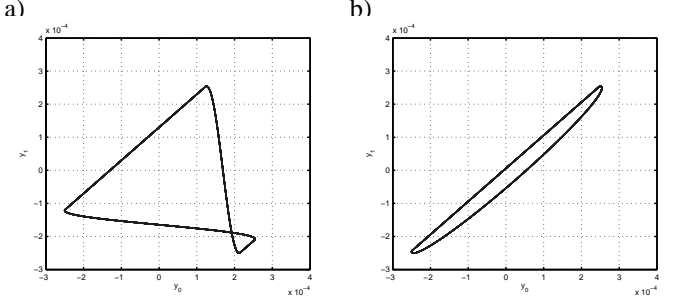


Figure 21. RECONSTRUCTIONS BASED ON TIME-LAG CRITERIA:
a) ZERO CROSSING OF C_{yy} ($i_1 = 1300$): INACCEPTABLE RESULT, SINCE TRAJECTORY INTERSECTS. b) MUTUAL INFORMATION ($i_2 = 60$): GOOD RESULT, SINCE STRUCTURE OF LIMIT-CYCLE IS PRESERVED (NO INTERSECTION, SHAPE QUALITATIVELY SIMILAR).

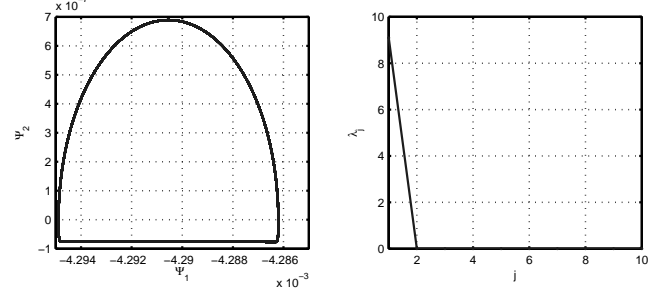


Figure 22. RECONSTRUCTION USING PCA: a) EXCELLENTLY RECONSTRUCTED LIMIT-CYCLE. b) SPECTRUM OF Σ .

gives a much better result: no intersection, only one straight line (stiction) and a reconstruction that is quite similar to the original phase-plot.

Eventually, the best result is obtained by the principle component analysis (cf. Fig. 22 a): apart from a rotation, the shape of the reconstruction perfectly matches the original limit-cycle, without any distortion or intersection. Figure 22 b) shows the corresponding ten eigenvalues of the covariance matrix Σ . It can be observed, that the spectrum is dominated by the first eigenvalue, while the remaining almost vanish: this may be interpreted to owe to the structure of the system, which during the motion changes from 1 DOF (2 state variable) to 0 DOF (1 state variable). Hence, it may be interpreted that the resulting eigenvalue spectrum gives only a kind of "averaged" system dimension.

Concluding, choosing the time delay with regard to the first minimum of the average mutual information and the reconstruction using the the principal components is supposed to give good results, even when analysing critical systems. Especially, the principal component analysis showed very good performance.